Magn Reson Mater Phy (2009) 22:71–76
DOI 10.1007/s10334-008-0143-1

RESEARCH ARTICLE

Sub-pixel localisation of passive micro-coil fiducial markers in interventional MRI

Marc Rea · Donald McRobbie · Haytham Elhawary · Zion T. H. Tse · Michael Lamperth · Ian Young

Received: 2 June 2008 / Revised: 26 August 2008 / Accepted: 28 August 2008 / Published online: 19 September 2008

Abstract
Objective Electromechanical devices enable increased accuracy in surgical procedures, and the recent development of MRI-compatible mechatronics permits the use of MRI for real-time image guidance. Integrated imaging of resonant micro-coil fiducials provides an accurate method of tracking devices in a scanner with increased flexibility compared to gradient tracking. Here we report on the ability of ten different image-processing algorithms to track micro-coil fiducials with sub-pixel accuracy.
Materials and methods Five algorithms: *maximum pixel, barycentric weighting, linear interpolation, quadratic fitting* and *Gaussian fitting* were applied both directly to the pixel intensity matrix and to the cross-correlation matrix obtained by 2D convolution with a reference image.
Results Using images of a 3 mm fiducial marker and a pixel size of 1.1 mm, *intensity linear interpolation*, which calculates the position of the fiducial centre by interpolating the pixel data to find the fiducial edges, was found to give the best performance for minimal computing power; a maximum error of 0.22 mm was observed in fiducial localisation for displacements up to 40 mm. The inherent standard deviation of fiducial localisation was 0.04 mm.
Conclusion This work enables greater accuracy to be achieved in passive fiducial tracking.

M. Rea (✉) · D. McRobbie
Radiological Sciences Unit (2N),
Charing Cross Hospital,
London, W6 8RF, UK
e-mail: marc.rea@imperial.ac.uk

M. Rea · H. Elhawary · Z. T. H. Tse · M. Lamperth · I. Young
Mechatronics in Medicine, Mechanical Engineering,
Imperial College London,
London, UK

Keywords MRI · Tracking · Localization · Fiducial markers · Imageprocessing

Introduction

Localization of instruments in MRI scanners is an area of current research which is closely linked to MRI-compatible robotics. Intravascular interventional procedures have previously been the main driving force behind research into device tracking, but there are many other emerging applications. One way to approach the problem is to use micro-coil fiducial markers; positional information can be acquired using either the magnetic gradient fields, or images containing the markers. The simplest methods rely on the visualization of passive markers made from susceptible materials (i.e. containing gadolinium [1] or dysprosium [2]), as well as biopsy needles filled with contrast material [3]. Such markers do not always produce good contrast with the background tissue, being dependent upon the imaging sequence and the overall signal.

Resonant micro-coil fiducial markers were first used for localization in the 1990's, and are increasingly being used to track devices within MRI scanners [4,5]. Most systems use active markers, small coils connected into a receive channel on the scanner which record position dependent signals. Connecting the fiducials directly to the scanner allows them to be detuned during the RF excitation. This ensures that they do not compromise images, but raises patient safety issues with the cabling, particularly for coils placed internally. Still, good results have been obtained in animal and phantom studies [6] with multiple applications of 1-D gradients [7,8] and also with parallel imaging [9]. A related method which does not raise the issues surrounding patient safety is optical decoupling of fiducials using fibre-optic

cable and a photoresistor [10]. While this method previously required operator intervention, modern scanners may provide programmable optical outputs.

Images received from the scanner allow the clinician to guide the instrument to the desired location. The instrument position may be drawn on the current image to help with this guidance. Real-time processing of the images allows automatic slice alignment through a feedback loop with the scanner [9]. This has been shown using limited 1-D projections to track devices in three dimensions [11].

Tracking of passive (unconnected) fiducials requires careful selection of a pulse sequence to ensure marker contrast. Previously, dual-flip angle gradient echo sequences have been used with a low flip angle for fiducial imaging and a larger excitation for anatomical imaging [12]. In the fiducial images, fiducials can be located simply by finding the maximum intensity pixel (MIPx), to an accuracy which is dependent upon the pixel dimension and the size of the fiducial. This is not sufficient for small, precise movements possible with electromechanical devices, and a suitable method of processing the images is required in order to achieve greater precision of fiducial centring. This work evaluates the accuracy of five suitable algorithms for tracking fiducials when applied to both an intensity matrix, and a cross-correlation matrix obtained by pre-processing with a reference image.

Methods

A fiducial coil was constructed by hand-winding 6 turns of 0.46 mm diameter enamelled wire around a 2.3 mm diameter cylindrical former. To allow fine-tuning, small gaps were left between the turns. The coil, with an inductance of around 55 nH, was soldered to a small piece of stripboard, and a non-magnetic capacitance of around 110 pF was connected in series to produce a resonance in the region of 64 MHz. To generate a signal, the coil was filled with a commercially-available vinyl plastisol gel (Dermal Pads, Spenco Healthcare, UK), which was cut into a cube of side 2 mm, forced into the coil and fixed with glue. The whole fiducial marker measured approximately $3\times3\times5$ mm. A network analyzer was then used to fine-tune the fiducial to 63.6 MHz by squeezing the coil, which was then fixed using epoxy resin (Superglue). The Q of the fiducial was around 60. The fiducial is shown in Fig. 1.

The fiducial was mounted on an MRI-compatible three degree of freedom (3-DOF) remote manipulator arm [13] as shown in Fig. 1. This device was placed into a Siemens Avanto 1.5T scanner, and the three axes were aligned with the scanner co-ordinate system using the positioning laser. All images were acquired with a fast low angle shot (FLASH) sequence (TE = 4.8 ms, TR = 9.2 ms, slice thickness 5 mm, matrix 256^2, FOV 280 mm, pixel size 1.1 mm, flip angle 1°, bandwidth 390 Hz/pxl) and an axial slice located at the isocentre. The translation of the arm inside the scanner was controlled by an independent control system using optical encoders, with an accuracy of 0.08 mm along each axis [13]. Exported images in DICOM format were later processed on a separate PC using MatLab (Mathworks, Natick, MA, USA). To obtain a base image and assess repeatability, 30 images were first acquired with the fiducial located at the isocentre of the scanner. These 30 images were averaged to obtain a reference image for later processing (see Fig. 2). The manipulator

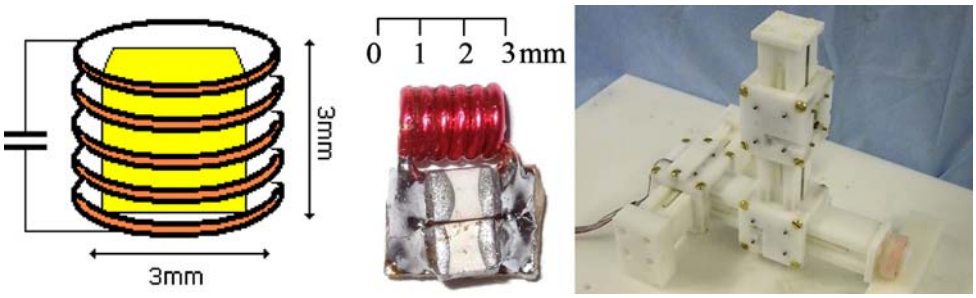

Fig. 1 Tuned micro-coil fiducial markers. *Left* diagram showing the dimensions of the coil and the placement of material. *Middle* an actual fiducial. *Right* the 3-DOF manipulator arm [13]

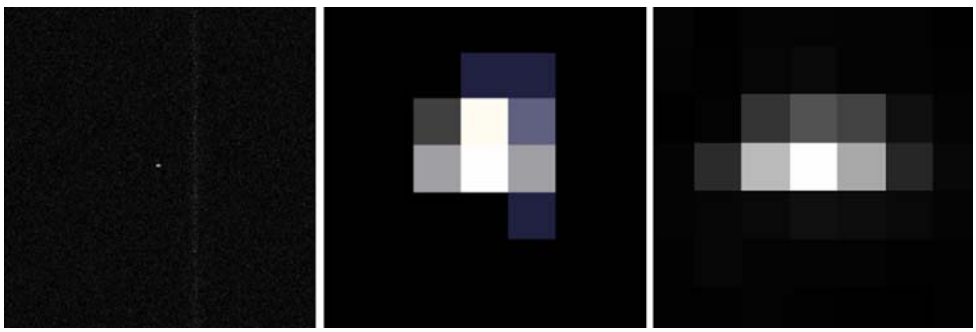

Fig. 2 Images of a single fiducial. *Left* a typical low-flip angle image. *Middle* an image of the 7×7 pixel submatrix centred on the MIPx. *Right* a reference image obtained by averaging the submatrices obtained from 30 measurements of the fiducial in the same location

was then translated various distances ranging from 0.1 to 40 mm in the x-direction. At each displacement five separate images were taken.

The imaging data were analysed using ten sub-pixel detection algorithms adapted from digital photography [14]. These algorithms were first combined into a MatLab program which applied each in turn and wrote the results to a separate text file.

The first five of the algorithms used only the image data from a single slice for positioning, while the other five required the reference image to calculate a cross-correlation co-efficient which was then used to determine a relative displacement. The cross correlation co-efficient is a measure of the similarity of two images or functions. It can be used in this context to transpose one image of a fiducial onto another. For two-dimensional digital images it is defined as:

$$C(u,v) = \frac{\sum_i \sum_j [f(x,y) - f_m][g(x+u, y+v) - g_m]}{\sqrt{\sum_{ij} [f(x,y) - f_m]^2 \sqrt{\sum_{ij} [g(x+u, y+v) - g_m]^2}}} \quad (1)$$

where i and j are the submatrix pixel indices, f_m and g_m are the mean values of the two image functions f and g, and u and v are pixel offsets in the x, y(i and j) directions.

To map the variation in the correlation coefficient, the sub-matrix of one image is passed across the other image in two dimensions, and at each alignment the correlation co-efficient of the pixels C, is determined. This produces a two dimensional matrix of the variation in C, which we shall call the C-matrix.

Before running the fiducial detection program, all of the images were pre-processed to remove any artifacts. This was done by recursively finding the MIPx and eliminating any that were:

- within three standard deviations of the mean. In this case it was assumed that the MIPx was noise, and there were no more fiducials present within the image.
- near the edge of the matrix. The fiducial should remain close to the centre of the image; if it was not, then the sub-matrix could not be correctly selected.
- not adjacent to another pixel with one third of the MIPx value. In this case it was assumed that the pixel was an artifact caused by a DC offset error in the ADC.

After correctly locating the fiducial in each image a sub-matrix of 7×7 pixels was taken for the sub-pixel processing. A typical submatrix is shown in Fig. 2. The ten algorithms are explained below.

Image processing algorithms

Intensity maximum pixel (IMP)—This algorithm simply searches for the MIPx and checks surrounding pixels for the same value. In the case of a single pixel, the fiducial centre is positioned at the centre of the pixel. For multiple pixels with the same value the position is placed midway between the similar pixels.

Intensity barycentric weighting (IBC)—This algorithm uses pixel intensity to weight each pixel in the submatrix to obtain a *centre-of-mass* type calculation of the fiducial position. The centre is given by:

$$x_m = \Sigma_i(x_i p_i)/\Sigma_i(x_i) \quad y_m = \Sigma_i(y_i p_i)/\Sigma_i(y_i) \quad (2)$$

where (x_m, y_m) is the calculated centre position, and p_i is the pixel intensity at (x_i, y_i).

Intensity linear interpolation (ILI)—This algorithm calculates the position of the centre of the fiducial from the mean position of the two edges. Intensity values passing through the MIPx in either through the horizontal or the vertical direction are taken (see Fig. 3), then interpolated to find the edges of the fiducial (taken as full width at half-maximum), and the mean of the two readings is taken to be the fiducial centre in that dimension. The method is then repeated for the other direction.

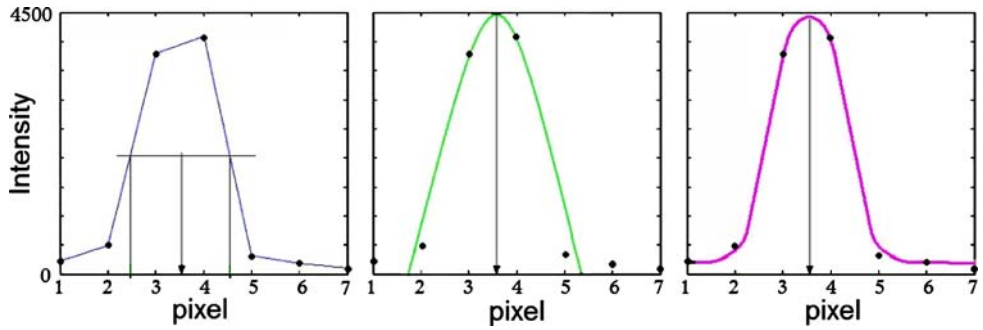

Fig. 3 1-Dimensional application of three of the algorithms to a vertical line drawn through the 7×7 submatrix in Fig. 2. The *dots* and *overlaid graph* show the intensity, the *arrow* shows how the centre of the fiducial is calculated. *Left* (ILI) the centre is found using the width at half-maximum. *Middle* (IQF) a quadratic curve is fitted using only the central pixels above the half-maximum threshold and the first pixels on either side. The centre is taken at the peak of the curve. *Right* (IGF) a Gaussian curve fitted to the data. The fiducial centre is taken at the peak

Intensity quadratic fitting (IQF)—the intensity quadratic curve fitting algorithm fits a bi-quadratic curve to the pixels in the submatrix around the MIPx. This second order fitting uses a least squares estimation of the error, and produces two sets of three coefficients that can be used to reconstruct the curve and find the maximum. The fitting process was greatly improved by using only the first pixels below the half-maximum threshold, since this removed the influence of pixels with only noise. The maximum of the reconstructed curve is taken as the centre of the fiducial (see Fig. 3).

Intensity gaussian fitting (IGF)—this is similar to IQF, but uses a 2D Gaussian curve to do the fit (see Fig. 3). The fit was recursively improved to a tolerance of $<10^{-5}$ which was chosen as it gave a good fit in reasonable time.

Each of the five algorithms above was then applied to the C-matrix in a similar manner:

Correlation-coefficient maximum pixel (CMP)
Correlation-coefficient barycentre weighting (CBC)
Correlation-coefficient linear interpolation (CLI)
Correlation-coefficient quadratic fitting (CQF)
Correlation-coefficient Gaussian fitting (CGF)

Results

The 30 images taken with the fiducial static at the isocentre were first analysed with each of the ten algorithms to obtain a standard deviation representing the inherent precision associated with the imaging procedure and each of the ten algorithms.

From the results shown in Table 1, it can be seen that the IMP algorithm produced good results for large movements, but as expected it could not produce a precision of less than 0.5 pixels. The IBC method was an improvement, but also showed signs of instability particularly at small distances. ILI was well-behaved even at small displacements. The quadratic curve fitting algorithm (IQF) was generally poor performing with an average error value well above those of the other algorithms, indicating that the curve fitting is not robust. IGF gave the smallest errors of all of the intensity matrix algorithms, although requiring much longer calculation times.

Of the five algorithms that employed the C-matrix, only CBC was found to give a large improvement over its counterpart Intensity matrix algorithm. For all C-matrix algorithms any gains in performance came at a cost of increased runtimes.

A summary of the results produced by application of all ten of the algorithms in the simulation is given in Table 1.

Discussion

The values in Table 1 demonstrate that the much-used method of IMP and its cross-correlation counterpart CMP are of little use at resolving fiducial locations to sub-pixel distances. The same can also be said for the fitting of quadratic curves (i.e. IQF, CQF) to data. The graphs in Fig. 4 show that of the six remaining algorithms, IBC is relatively unreliable and affected by image noise, yet there is little difference between the five algorithms ILI, IGF, CBC, CLI, and CGF. Overall ILI is a simple yet effective method of estimating the position of a fiducial; producing good results for all displacements with an inherent precision of 0.04 mm. This may be expected since it models the physical situation well, i.e. a homogenous uniform sample with a linear boundary. The IGF algorithm provided a slight improvement over ILI, and although the longer

Table 1 The performance of the tracking algorithms when using a 7×7 pixel sub-matrix

Algorithm	Std. dev. (mm)	Mean abs. error (mm)	RMS error (mm)	Maximum error (mm)	Approximate runtime (ms)
IMP	0	0.22	0.29	0.60	0.09
IBC	0.05	0.11	0.14	0.29	0.34
ILI	0.04	0.10	0.13	0.22	0.30
IQF	0.04	0.23	0.28	0.57	2.6
IGF	0.04	0.07	0.09	0.19	37.2
CMP	0.01	0.21	0.27	0.52	21.4
CBC	0.05	0.06	0.09	0.24	21.6
CLI	0.04	0.10	0.14	0.28	22.4
CQF	0.02	0.23	0.30	0.65	25.0
CGF	0.02	0.06	0.08	0.19	43.3

The first column shows the standard deviation of 30 repeated measurements with no translational movement. The mean absolute error, root mean square error and maximum error indicate the calculated positions against the optical encoder measurements for the full range of movements, and are shown with the. The approximate calculation times are also given per image slice

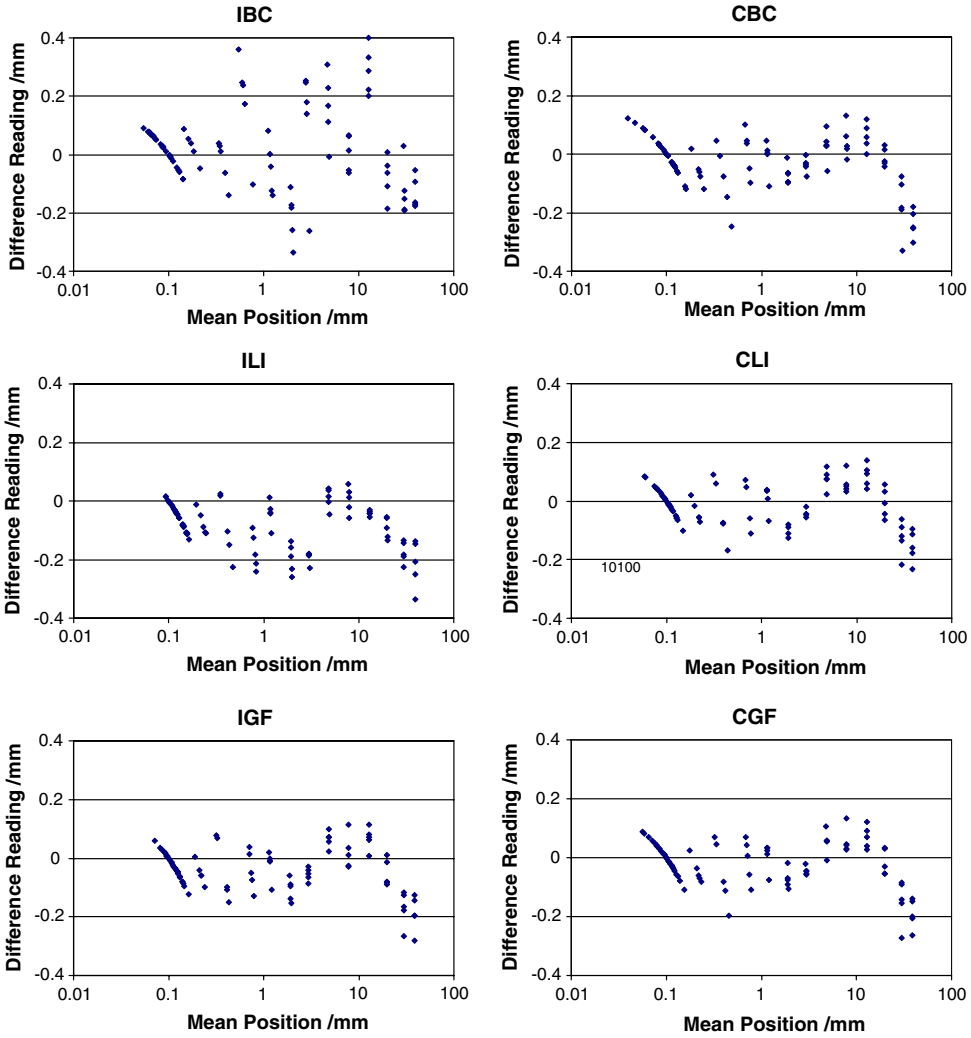

Fig. 4 Bland-Altman plots showing the performance of the six best-performing algorithms (IBC, ILI, IGF, CBC, CLI, CGF). Each *graph* shows the positional errors of the image processing algorithm for displacements of up to 40 mm along the *x*-axis, with each reading being referenced to the position of the optical encoders

computation times may limit its practicality, a compromise may be found by reducing the fitting tolerance.

Where time is not a factor, using a Cross-correlation matrix can provide even better results, although it is not known how the quality of the reference image used affects the performance. Interestingly, the calculation of the C-matrix has recently been shown to be greatly simplified by performing it in k-space, i.e. before FFT of the data [15]. This should reduce the time necessary to apply the C-matrix algorithms. However, use of the C-matrix introduces additional requirements such as obtaining the reference image and increasing the number of programming steps.

The stated 0.08 mm inherent accuracy of the optical encoders also meant that they were a significant source of error in the experiment, and while sufficient for most purposes they do not match the accuracy provided by sub-pixel fiducial tracking. The general trend of points in these five plots depicts a systematic error that may be attributed to readings taken from the optical encoders, most likely non-linearity of the printed reflective strips.

There are a number of additional factors which may affect the accuracy of fiducial positioning, the most obvious being non-linearity of the applied gradients which become more apparent further from the isocentre. The chemical shift of the Spenco material is less than 10 Hz at 1.5T which results in a constant positional offset of less than 0.03 mm at a bandwidth of 390 Hz/pixel. It was also found, when using such a high Q fiducial micro-coil and a 1° flip angle that the SNR is sufficient in all cases to easily resolve the marker against the background noise.

Conclusion

We have shown that the ILI algorithm is both sufficient, and computationally efficient for use in tracking passive micro-coil fiducials by image processing. A maximum error of 0.22 mm was achieved using ILI positional reconstruction with 3 mm coils and a matrix size of 1.1 mm. Further gains in accuracy may be obtained using more complex methods, but

at the cost of longer computation times and additional image requirements. This work provides a basis for real-time 3D tracking of electromechanical devices inside MRI scanners.

Acknowledgments This work was done with the Mechatronics in Medicine Laboratory, Mechanical Engineering, Imperial College London. It was funded by DH-NEAT Grant D 083.

References

1. Smits HFM, Bakker CJG (1998) Susceptibility-based catheter visualization. In: Adam G, Debatin JF (eds) Interventional magnetic resonance imaging. Springer, Berlin, pp 51–55
2. Omary RA, Unal O, Koscielski DS, Frayne R, Korosec F, Mistretta C, Strother C, Grist T (2000) Real-time MR imaging-guided passive catheter tracking with use of gadolinium filled catheters. J Vasc Intervt Radiol 11:1079–1085
3. Beyersdorff D, Winkel A, Hamm B, Lenk S, Loening SA, Taupitz M (2005) MR imaging—guided prostate biopsy with a closed MR Unit at 1.5 T: initial results. Radiology 234(2):576–581
4. Coutts GA, Gilderdale DJ, Chui M, Kasuboski L, DeSouza NM (1998) Integrated and interactive position tracking and imaging of interventional tools and internal devices using small fiducial receiver coils. Magn Reson Med 40(6):908–913
5. Burl M, Coutts G, Young IR (1996) Tuned fiducial markers to identify body locations with minimal perturbation of tissue magnetization. Magn Reson Med 36:491–493
6. Fink C, Bock M, Umathum R, Volz S, Zuhlsdorff S, Grobholz R, Kauczor H, Hallscheidt P (2004) Renal embolization: feasibility of magnetic resonance-guidance using active catheter tracking and intra-arterial magnetic resonance angiography. Invest Radiol 39(2):111–119
7. Dumoulin CL, Souza SP, Darrow RD (1993) Real-time position monitoring of invasive devices using magnetic resonance. Magn Reson Med 29:411–415
8. Krieger A, Susil RC, Menard C, Coleman JA, Fichtinger G, Atalar E, Whitcomb LL (2005) Design of a novel MRI compatible manipulator for image guided prostate. IEEE T Bio-med Eng 52(2):306–313
9. Bock M, Muller S, Zuehlsdorff S, Speier P, Fink C, Hallscheidt P, Umathum R, Semmler W (2006) Active catheter tracking using parallel MRI and real-time image reconstruction. Magn Reson Med 55:1454–1459
10. Wong EY, Zhang Q, Duerk JL, Lewin JS, Wendt M (2000) An optical system for wireless detuning of parallel resonant circuits. J Magn Reson Imaging 12(4):632–638
11. Flask C, Elgort D, Wong E, Shankaranarayanan A, Lewin J, Wendt M, Duerk JL (2001) A method for fast 3D tracking using tuned fiducial markers and a limited LPR-FISP sequence. J Magn Reson Imaging 14:617–627
12. Rea MA, McRobbie DW, Elhawary H, Tse ZT, Lampérth M, Young I (2008) A system for 3D real-time tracking of MRI-compatible devices by image processing. ASME-IEEE T Mech 13(3):379–382
13. Tse ZTH, Elhawary H, Zivanovic A, Rea MA, Paley M, Bydder G, Davies BL, Young I, Lampérth MU (2008) A 3 degree of freedom MR compatible device for magic angle related in vivo experiments. ASME-IEEE T Mech 13(3):316–324
14. Bing P, Hui-min X, Bo-qin X, Fu-long D (2006) Performance of sub-pixel registration algorithms in digital image correlation. Meas Sci Technol 17:1615–1621
15. de Oliveira A, Rauschenberg J, Beyersdorff D, Semmler W, Bock M (2008) Automatic passive tracking of an endorectal prostate biopsy device using phase-only cross correlation. Magn Reson Med 59:1043–1050